Detailed experimental and theoretical study of elastic scattering at intermediate energies in the electron-cesium system

G. Baum,* N. Pavlović, and B. Roth[†]
Fakultät für Physik, Universität Bielefeld, D-33615 Bielefeld, Germany

K. Bartschat and Y. Fang[‡]
Department of Physics and Astronomy, Drake University, Des Moines, Iowa 50311

I. Bray
School of Mathematical and Physical Sciences, Murdoch University, Perth 6150, Western Australia
(Received 26 March 2002; published 13 August 2002)

A series of measurements and calculations has been carried out for angle-differential elastic *e*-Cs scattering in the intermediate-energy region from 4 eV to 25 eV. The experiment used spin-polarized beams to obtain several spin-asymmetry functions and the relative cross section in the angular range from 40° to 140°. Two theoretical methods were used for the calculations: A nonrelativistic convergent close-coupling treatment, which can predict the differential cross section and the (spin) exchange asymmetry, and a semirelativistic *R* matrix with pseudostates approach, which also predicts nonvanishing results for two other asymmetries that require the presence of relativistic effects. Given the difficulty of the problem, the overall agreement between the experimental data and the theoretical predictions is very satisfactory.

DOI: 10.1103/PhysRevA.66.022705 PACS number(s): 34.80.Bm, 34.80.Nz

I. INTRODUCTION

Electron scattering from Cs atoms has received considerable attention over the past three decades, theoretically as well as experimentally. For this heavy open-shell target, not only electron exchange but also explicitly spin-dependent relativistic effects, with the spin-orbit interaction as the most important example, can be expected. As a result, Cs is the only alkali target for which nonzero values of angle-differential spin asymmetries other than the standard ''exchange asymmetry'' have been experimentally confirmed [1,2].

A benchmark comparison between experimental data and predictions from several different theoretical models, for an incident projectile energy of 3 eV, was presented in an earlier letter [2]. This low energy was chosen since it was judged as presenting approximately an equal challenge to both experimentalists and theorists, with the former generally preferring higher energies due to the performance of electron optical elements and the latter preferring lower energies where coupling effects are essentially restricted to a few strongly coupled channels. The overall conclusion of the 3-eV study was a generally good agreement between experiment and theoretical predictions from an eight-state semirelativistic Breit-Pauli *R*-matrix calculation [3] for the differential cross section (DCS), the exchange asymmetry, and two other spin asymmetries. Predictions based on the corresponding full-relativistic eight-state Dirac-Breit *R*-matrix calculation [4] qualitatively agreed with experiment as well, but apparently suffered from deficiencies in the structure description of the target. Finally, predictions from a nonrelativistic convergent close-coupling (CCC) model [5] also agreed well with experiment for the DCS and the exchange asymmetry. Thus, 25 years after Burke and Mitchell [6] initiated the discussion of spin-polarized electron scattering from heavy quasi-one-electron atoms, it became possible to compare experimental and theoretical benchmark data for several spin-asymmetry functions.

The present joint experimental and theoretical study is the systematic extension of our previous work to cover a wide range of incident energies between 4 eV and 25 eV. We attempt to provide a detailed comparison for a large set of experimental data with up-to-date theoretical models in this ''intermediate-energy regime,'' corresponding to incident projectile energies of approximately one to five times the ionization threshold. This energy region is well suited for such a project, as it is theoretically most challenging but allows for accurate measurements in the difficult spin-polarization experiments. Therefore, a stringent test of the correct understanding and description of the underlying physics is possible.

Given the difficulty of this problem, major progress in the experimental and theoretical methods over the past decade was essential to obtain the results presented in this work. On the experimental side, the development of techniques for producing highly spin-polarized beams of cesium atoms as well as highly spin-polarized electron beams allowed for the measurement of several spin asymmetries with sufficient precision. On the theoretical side, the immense increase of computational power led to significant advances in the numerical treatment of electron-atom scattering in general, with the

*Email address: baum@physik.uni-bielefeld.de
[†]Present address: Institut für Experimentalphysik, Heinrich-Heine-Universität, D-40225 Düsseldorf, Germany.
[‡]Present address: Center for Nanotechnology, University of Wisconsin–Madison, Madison, WI 53706.

most important improvements occurring in the aforementioned intermediate-energy regime. In this energy range, coupling between the discrete and the continuum part of the target spectrum can become very important and often may not be neglected in a numerical model if reliable results are to be obtained.

Before these developments, experimental angle-differential work on cesium had been scarce and was limited to unpolarized initial states. Gehenn and Reichert [7] measured the shape of the elastic differential cross section from 0.8 eV to 20 eV in the angular range from 30° to 150°. Klewer, Beerlage, and van der Wiel [8] measured the spin polarization and angular distribution of elastically scattered electrons for energies of 13.5, 20, and 25 eV between 40° and 115°. On the theoretical side, *R* matrix models with a few discrete states included in the close-coupling expansion [3,4,9–11] were limited to low incident energies, while perturbative approaches such as relativistic potential scattering [12], sometimes incorporated in a distorted-wave model [13], were expected to be only valid for relatively high incident energies.

The first theoretical attempt to treat *e*-Cs collisions using the convergent close-coupling method was undertaken by Bartschat and Bray [5] who used the nonrelativistic CCC method to predict the angle-differential cross section and the spin-exchange asymmetry, as well as angle-integrated elastic, excitation, and ionization cross sections. Recently, Bartschat and Fang [14] extended the *R* matrix with pseudostates (RMPS) method [15,16] to include relativistic effects. Their work, finally, allowed for a comparison between experimental data and theoretical predictions for the differential cross section and all three spin asymmetries measured by the Bielefeld experiment at low and intermediate energies.

This paper is organized as follows. In the following section, we describe the observables of interest for the present study and their connection to the scattering amplitudes and the collision dynamics. This is followed by sections summarizing some details of the apparatus and the description of the numerical methods. The results are presented and discussed in Sec. V, followed by conclusions and an outlook to possible future work on this collision system.

II. OBSERVABLES

Burke and Mitchell [6] analyzed spin-polarization effects in low-energy elastic scattering of electrons by quasi-one-electron *S*-state atoms, allowing for both electron exchange and relativistic (spin-orbit) effects. They found that six complex amplitudes (a_i) are needed to completely describe the collision. In terms of these amplitudes, they wrote the collision matrix as

$$\mathbf{M}=a_1+(\boldsymbol{\sigma}_1\cdot\hat{\mathbf{n}})a_2+(\boldsymbol{\sigma}_2\cdot\hat{\mathbf{n}})a_3+(\boldsymbol{\sigma}_1\cdot\hat{\mathbf{n}})(\boldsymbol{\sigma}_2\cdot\hat{\mathbf{n}})a_4 +(\boldsymbol{\sigma}_1\cdot\hat{\mathbf{p}})(\boldsymbol{\sigma}_2\cdot\hat{\mathbf{p}})a_5+(\boldsymbol{\sigma}_1\cdot\hat{\mathbf{q}})(\boldsymbol{\sigma}_2\cdot\hat{\mathbf{q}})a_6, \quad (1)$$

where the $\boldsymbol{\sigma}_i$'s are the Pauli spin matrices, $\hat{\mathbf{n}}$ is a unit vector normal to the scattering plane, and $\hat{\mathbf{p}}$ and $\hat{\mathbf{q}}$ are unit vectors in the collision plane. Denoting $\mathbf{k}$ and $\mathbf{k}'$ as the initial and final projectile momenta, $\hat{\mathbf{p}}$ points in the direction of $\mathbf{k}+\mathbf{k}'$ while $\hat{\mathbf{q}}$ is parallel to the momentum-transfer direction $\mathbf{k}-\mathbf{k}'$. All scattering parameters were expressed in terms of the above amplitudes. For our scattering geometry shown in Fig. 1, the spin-dependent differential cross section reads

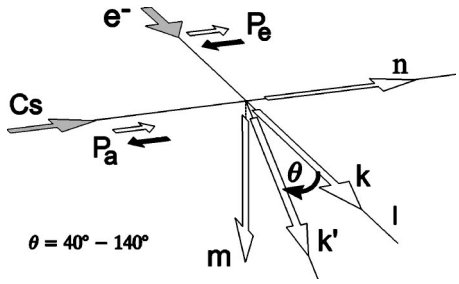

FIG. 1. Scattering geometry.

$$\sigma=\sigma_0[1+A_1(\mathbf{P}_a\cdot\hat{\mathbf{n}})+A_2(\mathbf{P}_e\cdot\hat{\mathbf{n}})-A_{nn}(\mathbf{P}_a\cdot\hat{\mathbf{n}})(\mathbf{P}_e\cdot\hat{\mathbf{n}})], \quad (2)$$

where σ_0 is the differential cross section for unpolarized beams, the A_i's are the observed spin asymmetries, and $\mathbf{P}_a$ and $\mathbf{P}_e$ are vectors describing the atomic and electron-spin polarizations, respectively.

Burke and Mitchell derived the following expressions for the relevant spin asymmetries:

$$A_1=2\ \mathrm{Re}(a_1a_2^*+a_3a_4^*)/\sigma_0,$$

$$A_2=2\ \mathrm{Re}(a_1a_3^*+a_2a_4^*)/\sigma_0, \quad (3)$$

$$A_{nn}=2\ \mathrm{Re}(-a_1a_4^*-a_2a_3^*+a_5a_6^*)/\sigma_0.$$

Here A_1 and A_2 correspond to single-spin ''up-down'' asymmetries (with respect to the reaction plane) of the DCS, either for scattering of unpolarized electrons from polarized atoms (A_1) or for scattering of polarized electrons from unpolarized atoms (A_2). Furthermore, A_{nn} represents a double-spin ''antiparallel-parallel'' asymmetry (with respect to the normal of the reaction plane) for scattering of polarized atoms from polarized electrons. In analogy to the nonrelativistic case, A_{nn} is often called an ''exchange asymmetry,'' but we note that not only the relative orientation of the projectile and target spins is relevant, but also their orientation with respect to the reaction plane [6]. Note that A_2 is identical to the Sherman function [17], i.e., it describes the left-right asymmetry in the differential cross section for scattering of spin-polarized electrons from unpolarized targets. Finally, as pointed out by Farago [18], nonvanishing values of A_1 require the simultaneous presence of spin-orbit and exchange effects, and hence this parameter is often called the ''interference asymmetry.''

A physical interpretation of the amplitudes can be obtained by examining the collision matrix of Eq. (1). The following types of interaction can be attributed to the different amplitudes:

a_1	Potential scattering
a_2	Spin-orbit scattering with exchange
a_3	Spin-orbit scattering
a_4	Potential scattering with exchange
a_5	Potential scattering with exchange, spins in direction $(\vec{\mathbf{k}}+\vec{\mathbf{k}}')$
a_6	Potential scattering with exchange, spins in direction $(\vec{\mathbf{k}}-\vec{\mathbf{k}}')$

Farago [19] showed that $a_2=a_4=a_5=a_6=0$ in the absence of exchange processes while $a_2=a_3=0$ and $a_4=a_5=a_6$ in the absence of spin-orbit interaction.

As seen from Eq. (3), all asymmetries contain only interference terms of amplitudes. The single-spin asymmetry connected with polarized atoms A_1 can be visualized as originating from the combined action of spin exchange via a_2 or a_4, thereby polarizing the incident electron beam, and nonexchange scattering via a_1 or a_3, respectively. The required spin-orbit interaction is provided either by the amplitude a_2 or by the amplitude a_3. The single-spin asymmetry connected with polarized electrons A_2 can be visualized as coming from the combined action of spin-orbit scattering via a_2 or a_3 and potential scattering via a_1 or a_4, respectively. The double-spin asymmetry A_{nn} originates from the interference of potential-scattering amplitudes involving exchange, either via a_4 or via a_5 and a_6. In addition, A_{nn} contains a contribution from the product of two spin-orbit amplitudes, $a_2 a_3^*$. This implies that, if potential scattering is dominant, contributions from relativistic spin-orbit effects to A_{nn} will be small.

Examining the asymmetries in Eq. (3) further for the case that there are spin-exchange effects but no spin-orbit effects present, one sees that only A_{nn} can be different from zero. If there are spin-orbit effects but no spin-exchange effects present, only A_2 can be different from zero. If there are, simultaneously, spin-exchange effects and spin-orbit effects present, all three asymmetries A_1, A_2, and A_{nn} may be different from zero, but we recall that a nonvanishing A_1 needs both exchange and spin-orbit effects. Not surprisingly, attempts to measure nonzero values of A_1 failed for the light sodium target [20], but they were indeed successful when using the heavier cesium target at the sufficiently low energy of 7 eV [1].

III. EXPERIMENT

A. Method

We use crossed beams of spin-polarized cesium atoms and spin-polarized electrons. The angle and energy of the scattered electron are selected with an energy analyzer rotatable in a plane perpendicular to the atomic beam. We determine the spin asymmetries by observing event yields for different combinations of projectile and target spin orientations. Specifically, we produce beam polarizations perpendicular to the reaction plane and measure four spin-dependent differential cross sections relative to each other by observing the count rates $N^{\uparrow\uparrow}$,$N^{\downarrow\downarrow}$,$N^{\uparrow\downarrow}$, and $N^{\downarrow\uparrow}$, where the first superscript indicates the target spin while the second denotes the projectile spin direction with respect to the scattering plane. From the accumulated, background corrected rates we construct ''raw asymmetries'' by forming suitable combinations of spin-dependent settings exploiting Eq. (2). Finally, A_1,A_2, and A_{nn} are obtained by normalizing to unity spin polarizations P_a, P_e, and P_aP_e, respectively. Specifically,

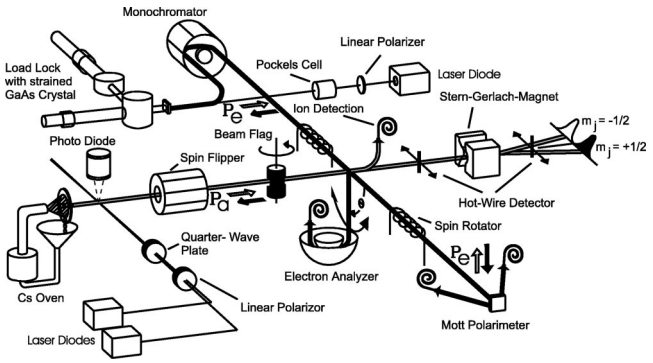

FIG. 2. Schematic diagram of the experimental setup.

$$A_{nn}=\frac{1}{P_aP_e}\frac{(N^{\uparrow\downarrow}+N^{\downarrow\uparrow})-(N^{\uparrow\uparrow}+N^{\downarrow\downarrow})}{(N^{\uparrow\downarrow}+N^{\downarrow\uparrow})+(N^{\uparrow\uparrow}+N^{\downarrow\downarrow})}, \tag{4}$$

$$A_2=\frac{1}{P_e}\frac{(N^{\uparrow\uparrow}+N^{\downarrow\uparrow})-(N^{\uparrow\downarrow}+N^{\downarrow\downarrow})}{(N^{\uparrow\uparrow}+N^{\downarrow\uparrow})+(N^{\uparrow\downarrow}+N^{\downarrow\downarrow})}, \tag{5}$$

$$A_1=\frac{1}{P_a}\frac{(N^{\uparrow\downarrow}+N^{\uparrow\uparrow})-(N^{\downarrow\downarrow}+N^{\downarrow\uparrow})}{(N^{\uparrow\downarrow}+N^{\uparrow\uparrow})+(N^{\downarrow\downarrow}+N^{\downarrow\uparrow})}. \tag{6}$$

In the determination of A_2, an unpolarized atomic beam is simulated by taking the average of $N^{\uparrow\uparrow}$ and $N^{\downarrow\uparrow}$ for electrons with spin ''up'' and of $N^{\uparrow\downarrow}$ and $N^{\downarrow\downarrow}$ for electrons with spin ''down,'' respectively. Similar averages are taken to simulate an unpolarized electron beam for the measurement of A_1. For the relative measurement of the differential cross section σ_0, we actually used unpolarized beams. The schematic diagram of our experimental arrangement is shown in Fig. 2.

B. Atomic beam

The spin-polarized atomic beam was described in detail before [21]. It is produced from a recirculating Cs oven, which is reloadable under vacuum after 200 h continuous operating time. For polarizing we use optical pumping with two laser diodes in single-mode operation, tuned to transitions from both hyperfine levels of the ground state. A spin flipper in front of the scattering chamber allows for reversal of the atomic beam polarization and is also used for determination of the polarization. We typically obtained a polar-

ization of $P_a = 0.85$, as measured with a Stern-Gerlach magnet, at an atomic beam density of $5 \times 10^9/\mathrm{cm}^3$ in the scattering center. The relative uncertainty in the polarization measurement for the different experiments ranged from $\delta P_a / P_a = \pm 4.5\%$ to $\delta P_a / P_a = \pm 8.5\%$.

C. Electron beam

The spin-polarized electron beam is produced by photoemission from a strained GaAs crystal [22] using light from a GaAlAs laser diode operating at a wavelength of 850 nm. A Pockels cell is used for generating either right-hand or left-hand circularly polarized light, leading to a transverse spin direction either parallel or antiparallel to $\hat{\mathbf{n}}$. Electron optical elements in front of and behind the collision region ensure a proper guiding of the electron beam with the main purpose of avoiding high background count rates. With the strained crystal we obtain currents of 0.5 μA in the scattering region and a typical polarization of $P_e = 0.65$, as measured with a retarding field Mott polarimeter. The relative uncertainty in the polarization measurement amounts to $\delta P_e / P_e = \pm 4.5\%$. The 180° electrostatic monochromator with a central radius of 10 cm is set to provide an energy spread of $\Delta E = 150$ meV in the beam.

D. Scattering region

In the scattering chamber, the hemispherical electron energy analyzer is located below the plane of the two horizontal crossed beams and can be rotated around the atomic beam axis, for scattering angles between 40° and 140°. The analyzer has a central radius of 3.3 cm and is operated with a resolution of typically $\Delta E/E = 5\%$ to select elastically scattered electrons. The five-element electron optical lens system at the entrance to the analyzer defines the accepted phase space, as determined with an electron-optical simulation program. In the course of our investigations, we noticed that we could not always reproduce the shape of the DCS as measured by Gehenn and Reichert [7]. This was traced back to the influence of a beam-beam related background originating from electrons scattered by the atomic beam with high rate into the forward direction. We eliminated this adverse effect by installing an additional collimator in the lens system of the analyzer, by increasing the distance of the electron-optical elements of the electron beam from the scattering center, and by relying upon results of electron ray tracing to find settings with a favorable form of the accepted phase space. From this we determined the angular resolution of the analyzer and found for $\Delta\theta_{\mathrm{FWHM}}$ (where FWHM is full width at half maximum) the following values: 11° at 4 eV, 8° at 20 and 25 eV, 6° at 5 and 15 eV, 5° at 6, 7, 8, 10, and 18 eV, 4° at 9 and 13 eV.

Finally, an ion detector is installed near the scattering center to monitor the production of Cs^+ ions by scanning the projectile energy in the vicinity of the ionization threshold at 3.9 eV. We can observe the onset of ionization with an accuracy of ± 0.1 eV and use it to calibrate the energy scale. In addition, comparing the observed spin asymmetry in the total ionization cross section with our earlier measurements [23] gives an easy and fast cross-check on the correct spin settings, particularly regarding the collinearity of P_a and P_e. Furthermore, the spin settings are alternated in short-time intervals to reduce systematic errors, and determinations of background rates are interspersed by shutting off the atomic beam with the beam flag.

IV. THEORY

A. Target structure

The first problem arising in the numerical treatment of electron collisions with many-electron targets is a proper description of the target structure. For Cs, in particular, the two primary choices are either an ''all-electron'' model or a ''quasi-one-electron'' approach. The latter choice is motivated by the fact that our interest is focused on the interaction between the projectile and the valence electron. Based on early work of Norcross [24], an accurate, though still manageable (in a subsequent collision calculation) target description can be obtained by including a semiempirical core potential to describe the response of the target core to the valence target electron and the incident projectile. In fact, Thumm and Norcross [10] showed that modifying this potential even further, by including a dielectric term to account for the simultaneous effect of both outer electrons on the core, was essential at very low incident energies. Furthermore, calibrating the strength of the spin-orbit interaction in a perturbative treatment with nonrelativistic orbitals, using the experimentally known bound spectrum as a guide, provides results of comparable accuracy to what is typically obtained in *ab initio* full-relativistic structure calculations.

The core-potential approach, modeling both core polarization and exchange between the outer electrons and the core [25], was used in the semirelativistic RMPS calculations by Bartschat and Fang [14] to obtain physical as well as pseudoorbitals (see below). In fact, their results indicated the crucial role of a suitable core potential, particularly at relatively high incident energies, where channel coupling loses importance relative to the description of the target structure. Remaining deficiencies in that target description, rather than channel-coupling or relativistic effects, were found to be the principal reason for the discrepancies between the early CCC predictions [5] and the measurements at an incident energy of 20 eV [14].

The CCC calculations reported in the present paper were carried out with a target description that uses a Hartree-Fock core potential together with a core-polarization potential with values of $\alpha_d = 15.644 a_0^3$ for the dipole polarizability of the core and $\rho = 2.05 a_0$ as the cutoff radius (see Ref. [26] for details).

B. Collision calculations

As mentioned above, the channel coupling between a large number of discrete states and the ionization continuum can become extremely important for the treatment of atomic collisions in the intermediate-energy regime. In the CCC

approach of Bray and Stelbovics [27,28], as well as in closely related treatments such as the RMPS method [15,16], an attempt is made to account for the channel coupling effect, ideally to convergence, by including a sufficiently large number of physical states together with ''pseudostates'' in the close-coupling plus correlation expansion. The latter states approximate the coupling to both the high-lying discrete and the continuum states of the target that are not included explicitly.

The RMPS calculations were described in detail by Bartschat and Fang [14]. Briefly, 8-state, 24-state, and 40-state calculations were performed, constructed by adding a valence electron to the closed Xe-like core of Cs^+. In the 40-state Breit-Pauli *R*-matrix model (labeled BP40 below) the valence electron was allowed to occupy one of the physical orbitals $(6s,6p,5d,6s,7p)$ or one of the pseudo-orbitals $\overline{8}s$-$\overline{12}s$, $\overline{8}p$-$\overline{12}p$, $\overline{6}d$-$\overline{10}d$, or $\overline{4}f$-$\overline{5}f$. Relativistic effects were included via the one-body spin-orbit term of the Breit-Pauli Hamiltonian, while the spin-conserving mass correction and Darwin terms were incorporated indirectly in the optimization procedure of the model potential [25]. Because of the fine-structure levels and the relativistic coupling scheme used in this model, the BP40 calculation contained up to 178 coupled channels, leading to many Hamiltonian matrices of dimensions above 5000 to be diagonalized in setting up the *R*-matrix basis. In addition to the computational effort, it was also necessary to carefully watch the numerical details when coupling a large number of nearly though not exactly degenerate channels.

The nonrelativistic CCC calculations were performed using the formalism specified in Ref. [26]. As above, the maximum value of target state orbital angular momentum ($l_{\max}$) was set to 3. In order to achieve a good description of the lowest eigenstates the Laguerre bases were defined with $N_l = 65 - l$ and exponential falloffs $\lambda_l \approx 6$. For energies above the ionization threshold, a slight variation in the λ_l was used to ensure that the total energy fell half-way between two pseudothresholds. This procedure generated an adequate representation of the discrete spectrum, but too many positive-energy pseudostates to use in scattering calculations. Fortunately, because the highest energy considered in this work is 25 eV, keeping all energetically open states and just two closed ones for each *l* resulted in practically feasible calculations. The largest, for 25 eV, used a total of 72 states, whereas the smallest calculation included 31 states. For comparison, the BP40 model would correspond to 23 coupled states in a nonrelativistic scheme.

V. RESULTS

Figures 3 –5 present our results for the angle-differential cross section σ_0 and the spin asymmetries A_{nn}, A_2, and A_1 for elastic electron scattering from Cs atoms at incident electron energies between 4 eV and 7 eV (Fig. 3), 8 eV and 13 eV (Fig. 4), and 15 eV and 25 eV (Fig. 5). The relative experimental results for the cross section have been normalized to give a good visual fit to the theoretical predictions. When possible, the experimental data from the current work are compared with the relative cross-section results of Gehenn and Reichert [7] and with the data of Klewer *et al.* [8] for the DCS and the spin asymmetry A_2. Only the BP40 and the current CCC predictions are shown since we judge them to be our two best models. The effect of reducing the number of coupled channels was discussed for three representative energies by Bartschat and Fang [14].

Our experimental data points only show the statistical error bars. Systematic errors originate from uncertainties in the determination of the polarizations which are added in quadrature for the product of P_a and P_e. For the asymmetries, these errors typically amount to $\pm 9\%$ for A_{nn}, $\pm 4.5\%$ for A_2, and $\pm 8\%$ for A_1. Note that these are scale uncertainties, i.e., the absolute error is proportional to the size of the asymmetry itself. The influence of the finite angular resolution of the electron detector on the results can be taken into consideration by convoluting the theoretical data with the experimental resolution function for the comparison. It was found that for all energies with $\Delta\theta_{\mathrm{FWHM}} < 5°$ this is an insignificant effect. Only where $\Delta\theta_{\mathrm{FWHM}} > 5°$ and where the theoretical structures are sharp, the convoluted values are noticeable changed. Examples are discussed in the text below.

As seen from Fig. 3, the agreement between the experimental data and the semirelativistic RMPS predictions is in general very satisfactory for the differential cross section and all three spin asymmetries, except for the incident energy of 7 eV. Furthermore, the nonrelativistic CCC model predicts σ_0 and A_{nn} very well for all energies, including 7 eV. This finding indicates that relativistic effects can apparently be omitted if one is only interested in these two ''nonrelativistic'' parameters.

Looking in more detail at the 4-eV data, the BP40 prediction for A_{nn} exhibits a relative broad structure near the forward ($\theta \approx 45°$) cross-section minimum. Convoluting with the finite experimental angular resolution reduces the asymmetry value here from $+0.44$ to $+0.41$, still staying in conflict with the experimental data and the CCC results. Near the backward ($\theta \approx 130°$) cross-section minimum, however, the sharp peak predicted by BP40 for A_{nn} is substantially reduced by the convolution procedure and then results in perfect agreement with experiment. For A_2, good agreement exists between experiment and the BP40 results, except for backward-scattering angles where the experiment gives asymmetry values about twice those predicted by theory. The measured spin asymmetry A_1 shows relative large values at this energy when compared to the other energies studied in this work. Nearly perfect accord with the BP40 results is found in both size and angular dependence of A_1 at this energy.

Going to 7 eV, the DCS from the BP40 calculation starts to show deviations (around 30° and 85°) from the good agreement between the experiments and the theories before. These deviations increase with energy and start to appear also for A_{nn}. However, good agreement of the BP40 data with experiment can still be stated for A_{nn} at 7 eV, and likewise for the CCC results. In contrast, the BP40 predictions for A_2 show a strong discrepancy with experiment around 80°, and discrepancies, though less pronounced, also exist

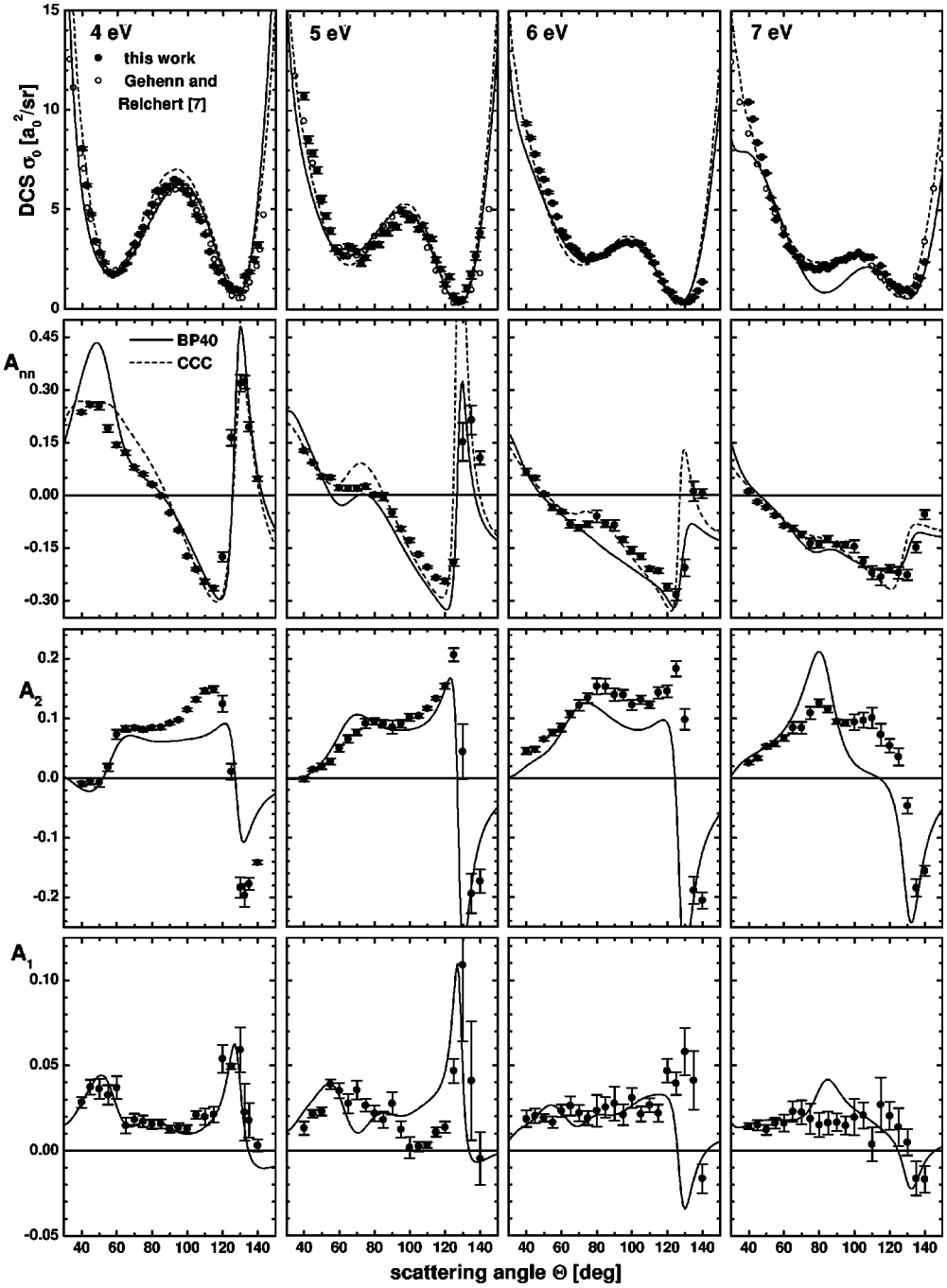

FIG. 3. Angle-differential cross section σ_0 and the spin asymmetries A_{nn}, A_2, and A_1 for elastic electron scattering from Cs atoms at incident electron energies of 4, 5, 6, and 7 eV. The relative experimental results for the cross section have been normalized through an optical fit to the theoretical predictions. The solid line represents the results from a 40-state Breit-Pauli *R*-matrix model (BP40) while the dashed line (only for σ_0 and A_{nn}) represents the nonrelativistic CCC results.

for A_1. The measured asymmetries differ slightly from the earlier data [1], because of the improvements in background handling (see Sec. III D).

Looking at Fig. 4, it is likely that the BP40 model, in this theoretically most challenging energy regime, still has convergence problems with respect to the number of states included in the close-coupling expansion. Except for large angles at 8 eV and at 13 eV overall, the CCC predictions for the differential cross section and the exchange asymmetry A_{nn} agree very well with the experimental data, whereas the RMPS curves exhibit some structures that are not seen experimentally. Nevertheless, it is worth noting that the BP40 model agrees at least qualitatively with the experimental results for the ''relativistic'' asymmetries A_1 and A_2 for which nonrelativistic models as CCC predict exactly zero values. Certainly noteworthy is the discrepancy between the experiments and the theories at 13 eV for the forward minimum (around 60°) of the DCS.

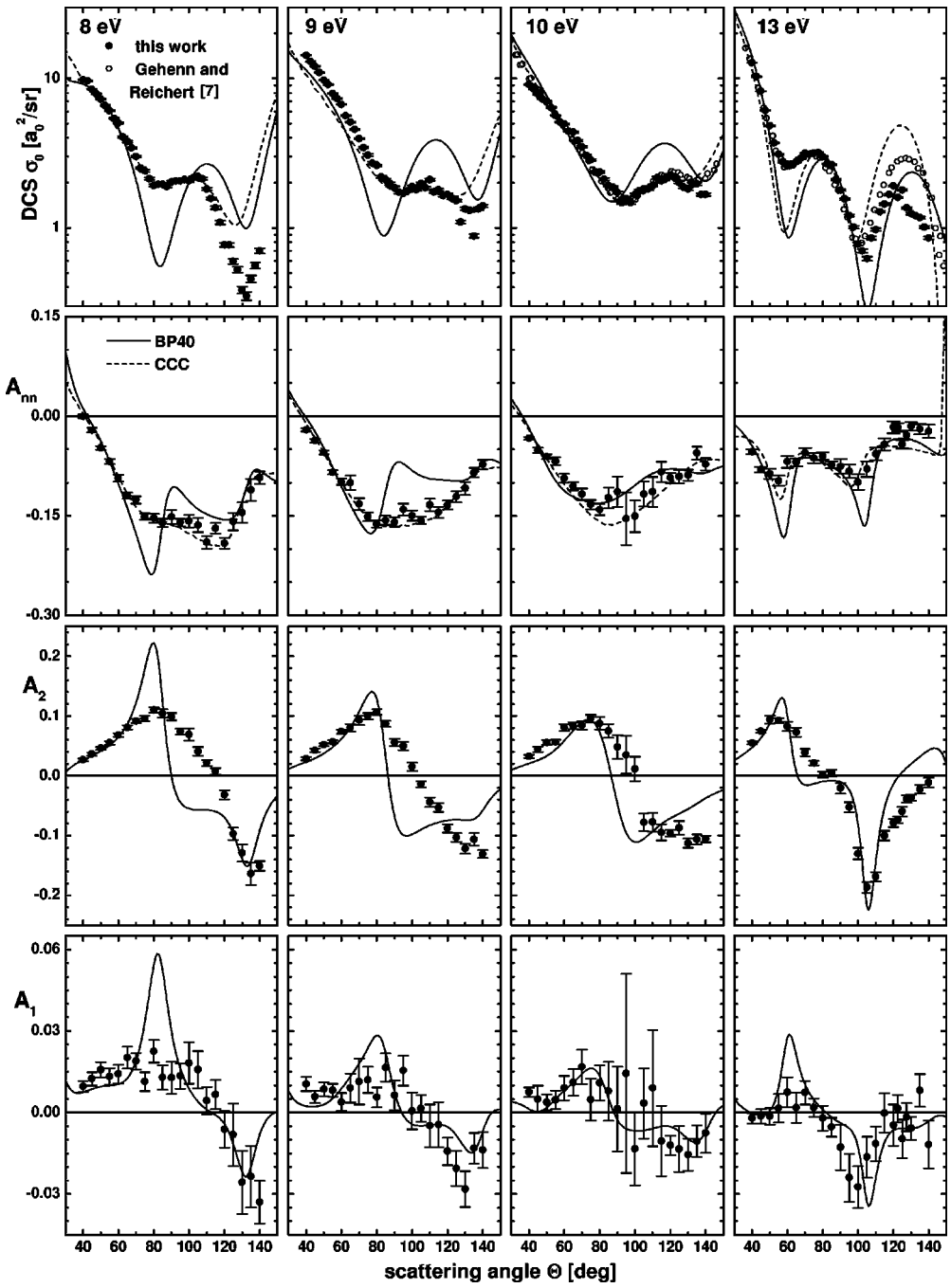

FIG. 4. Same as Fig. 3 for electron energies of 8, 9, 10, and 13 eV.

Moving to the last set of data exhibited in Fig. 5, we see that the predicted structures become sharper in their angular dependence, as is typically the case with increasing energy. For 15 eV, in particular, we note a very strong dependence of A_{nn} on the details of the theoretical model, with the experimental data tending towards the RMPS results for the sharp structure near 60° but clearly favoring the CCC predictions near 110°. It should be noted, however, that the latter sharp structure is reduced to essentially a zero asymmetry value after convolution with the finite angular resolution of $\Delta\theta_{\mathrm{FWHM}}=6°$. For the same reason, the cross-section minimum in the BP40 curve near 110° is lifted by nearly an order of magnitude, but even thereafter still drops an order of magnitude below the experimental minimum. In comparison, this minimum in the DCS predicted by the CCC model is not as deep and sharp. When going to larger scattering angles, the CCC results here agree very well with the measurements of Ref. [7]. Finally, as expected and well known from classic Mott scattering [17], we note that the spin-orbit asymmetry A_2 deviates further and further from zero near the cross-

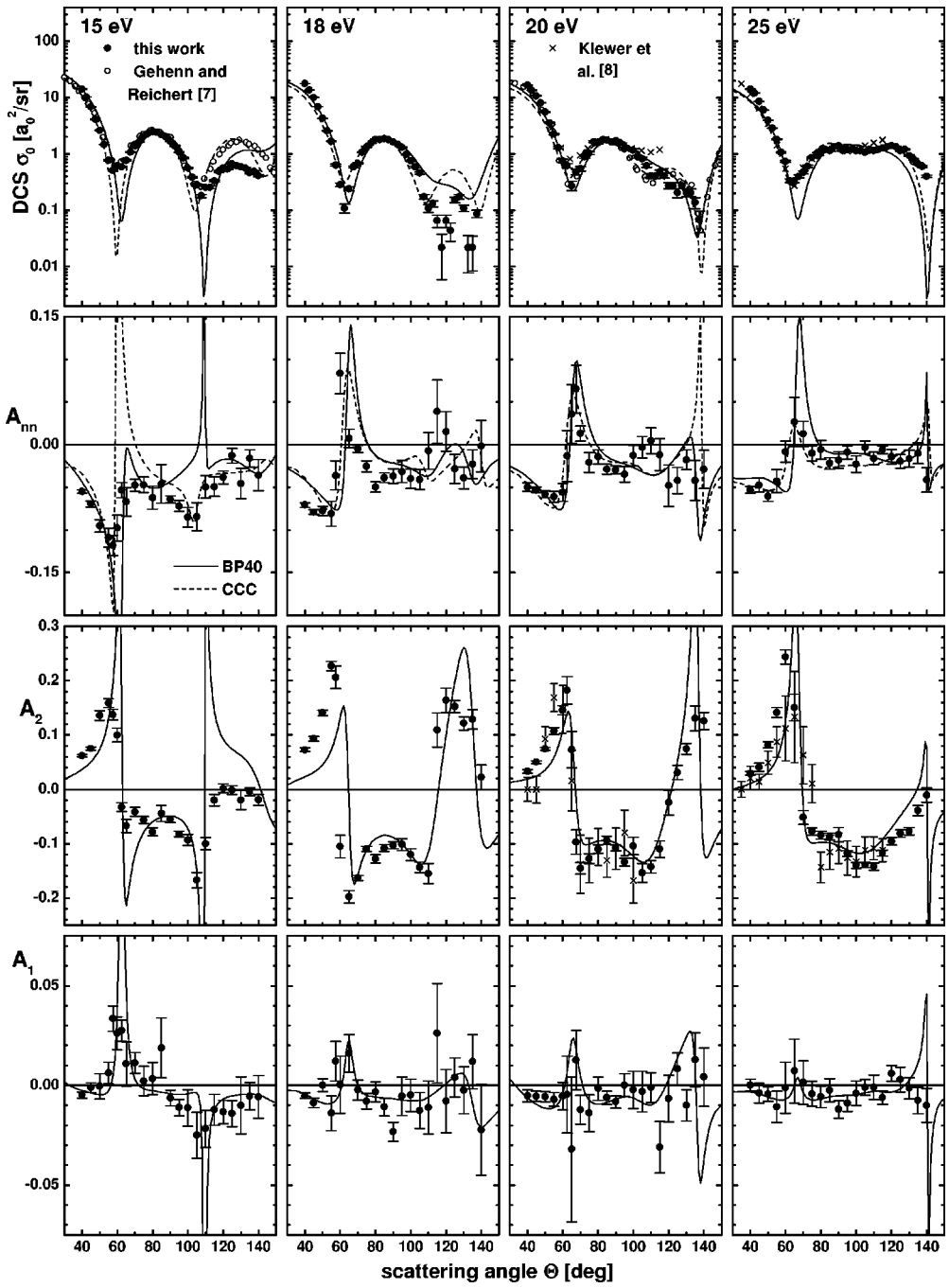

FIG. 5. Same as Fig. 3 for electron energies of 15, 18, 20, and 25 eV.

section minima, while the exchange asymmetry A_{nn} decreases overall and the spin-orbit and exchange asymmetry A_1 is hard to distinguish from zero for incident energies above 15 eV.

VI. CONCLUSIONS AND OUTLOOK

In this joint experimental and theoretical study, we have presented a set of benchmark data for spin-dependent elastic electron scattering from cesium atoms at incident electron energies between 4 eV and 25 eV for scattering angles between 30° and 150°. The overall agreement between the experimental data and the semirelativistic RMPS predictions is very satisfactory for electron energies below 7 eV and above 15 eV, indicating once again the challenge for theory in the intermediate-energy regime. Interestingly, the nonrelativistic CCC method can predict the parameters σ_0 and A_{nn} very well over nearly the complete range, with some exceptions at 8 eV, 13 eV, and 15 eV. Hence, for the calculation of these ''nonrelativistic'' parameters only, the inclusion of relativistic effects can apparently be traded off in favor of including a very large number of coupled channels.

We are currently in the process of extending our studies to inelastic collisions, particularly the optically allowed transitions $(6s)^2S_{1/2} \rightarrow (6p)^2P^o_{1/2,3/2}$. Based on theoretical predictions for the size of the DCS, it may also be possible to perform the experiment for the optically forbidden transitions $(6s)^2S_{1/2} \rightarrow (5d)^2D_{3/2,5/2}$. Preliminary data are very encouraging and the results will be presented in forthcoming publications.

ACKNOWLEDGMENTS

This work was supported in part by the Deutsche Forschungsgemeinschaft (G.B.,N.P.,B.R.), the National Science Foundation (K.B. and Y.F.), the Australian Research Council, and the Merit Allocation Scheme on the National Facility of the Australian Partnership for Advanced Computing (I.B.).

[1] B. Leuer *et al.*, Z. Phys. D: At., Mol. Clusters **33**, 39 (1995).
[2] G. Baum *et al.*, Phys. Rev. Lett. **82**, 1128 (1999).
[3] K. Bartschat, J. Phys. B **26**, 3595 (1993).
[4] S. Ait-Tahar, I. P. Grant, and P. H. Norrington, Phys. Rev. Lett. **79**, 2955 (1997).
[5] K. Bartschat and I. Bray, Phys. Rev. A **54**, 1723 (1996).
[6] P. G. Burke and J. F. B. Mitchell, J. Phys. B **7**, 214 (1974).
[7] W. Gehenn and E. Reichert, J. Phys. B **10**, 3105 (1977).
[8] M. Klewer, M. J. M. Beerlage, and M. J. van der Wiel, J. Phys. B **12**, L525 (1979).
[9] E. Karule, J. Phys. B **5**, 2051 (1972).
[10] U. Thumm and D. W. Norcross, Phys. Rev. Lett. **67**, 3495 (1991); Phys. Rev. A **45**, 6349 (1992); **47**, 305 (1993).
[11] U. Thumm, K. Bartschat, and D. W. Norcross, J. Phys. B **26**, 1587 (1993).
[12] D. W. Walker, J. Phys. B **7**, L489 (1974).
[13] V. Zeman, R. P. McEachran, and A. D. Stauffer, J. Phys. B **27**, 3175 (1994); **28**, 1835 (1995); **28**, 2781 (1995); **28**, 3063 (1995).
[14] K. Bartschat and Y. Fang, Phys. Rev. A **62**, 052719 (2000).
[15] K. Bartschat, E. T. Hudson, M. P. Scott, P. G. Burke, and V. M. Burke, J. Phys. B **29**, 115 (1996).
[16] K. Bartschat, Comput. Phys. Commun. **114**, 168 (1998).
[17] J. Kessler, *Polarized Electrons*, 2nd ed. (Springer, Heidelberg, 1985).
[18] P. S. Farago, J. Phys. B **7**, L28 (1974).
[19] P. S. Farago, in *Electron and Photon Interaction with Atoms*, edited by H. Kleinpoppen and M. R. C. McDowell (Plenum, New York, 1976), p. 235.
[20] J. J. McClelland *et al.*, J. Phys. B **23**, L21 (1990).
[21] G. Baum *et al.*, Z. Phys. D: At., Mol. Clusters **22**, 431 (1991).
[22] R. Prepost and T. Maruyama, Annu. Rev. Nucl. Part. Sci. **45**, 411 (1995).
[23] G. Baum *et al.*, J. Phys. B **26**, 331 (1993).
[24] D. W. Norcross, Phys. Rev. Lett. **32**, 192 (1974).
[25] B. J. Albright, K. Bartschat, and P. R. Flicek, J. Phys. B **26**, 337 (1993).
[26] I. Bray, Phys. Rev. A **49**, 1066 (1994).
[27] I. Bray and A. T. Stelbovics, Phys. Rev. A **46**, 6995 (1992).
[28] I. Bray and A. T. Stelbovics, Adv. At., Mol., Opt. Phys. **35**, 209 (1995).